Oxidation of Metals, Vol. 68, Nos. 1/2, August 2007 (© 2007)
DOI 10.1007/s11085-006-9048-4

Study of the Cyclic Oxidation Resistance of Superalloy IN-625: Lifetime Predicted by COSP-Modelling Program

E. N'dah,[*] M. P. Hierro,[*] K. Borrero,[*] and F. J. Pérez[*]

Received June 23, 2006; revised October 18, 2006

Cyclic-oxidation tests were performed on IN-625 in order to evaluate its oxidation resistance. IN-625 showed a strong cyclic-oxidation resistance at 900°C. At 1000°C, there was evaporation of chromium oxide leading to Cr depletion due to a reoxidation effect. Long-term exposure leads to microstructural modification; it seems to be detrimental. The chromia scale losses its protective properties and then IN-625 exhibits lower cyclic-oxidation resistance. The computer simulation by the COSP model, after 1000 cycles, predicts good cyclic -oxidation resistance of IN-625 at 900°C.

KEY WORDS: cyclic oxidation; chromia oxide; chromium manganese spinel; evaporation; spallation; simulation; COSP program.

INTRODUCTION

Nickel- base superalloys are widely used as turbine-blade components in aero and industrial gas turbines, because they combine good mechanical properties with microstructural stability at relatively high temperature.[1,2] They present not only good mechanical properties, such as stress rupture and fatigue resistance, but may exhibit good oxidation and hot-corrosion

*Facultad de Ciencias Químicas, Departamento de Ciencia de los Materiales, G.I. Ingenieria de Superficies UCM No. 910627, Universidad Complutense de Madrid, Madrid, 28040, Spain; e-mail: fjperez@quim.ucm.es

resistance.[3,4] Their mechanical properties can be retained by using nickel–chromium as a coating.[5] These alloys contain oxidizable elements which promote the external formation of stoichiometric protective oxides that act as a protective layer.[6] There are many different factors which influence blade lifetime. The blade can suffer from service-induced degradation which may be natural or accelerated due to different causes such as operation environment, high mechanical stresses, high thermal stresses, etc.[7]

Superalloys, such as Inconel 625, are well known as strong corrosion-resistant alloys. Their stability in the molten-carbonate fuel cells (MCFCs) environments, in reducing fuel and oxidant gas atmospheres, was studied by Jian et al.[8] They showed that Inconel 625 has sufficient oxidation resistance in the oxidant atmosphere of the MCFC at temperature around 650°C. It would be interesting to investigate the oxidation resistance at higher temperature for the process design and application of this alloy.

Many applications of high-temperature materials require repeated heating and cooling cycles. Materials which resist against mechanical damage under these conditions present more interest. During cooling, large compressive stresses arise in scales because the thermal-expansion coefficients of the substrate metals are greater than those of the oxides. This results in scale cracking, buckling, or delamination, and some degree of spallation. Many parameters, i.e. maximum and minimum temperature, cooling and heating rate, surface preparation, material composition, hold time, play an important role during cyclic oxidation.[1,9–12] Generally cyclic-oxidation, weight-change curves exhibit a basic shape consisting of an initial weight gain to a maximum value, a decrease followed by crossover to negative weight change, and finally a nearly linear rate of weight loss.[13,14] The total amount of material consumed is a complex function of the growth kinetics and degree of spallation, which therefore usually eludes an analytical solution.[15] Many studies devoted to modelling the iterative growth and spallation processes have been done for better understanding the cyclic-oxidation behavior of high-temperature materials. One of the models used is Cyclic Oxidation Spalling Program (COSP) developed by Smialek et al.[11] This model is focused on uniform spallation of an outer layer of the adherent scale, prescribing that the weight fraction of spalled oxide was a linear function of the retained oxide weight.[14,16] If F is the fraction of oxide spalled per cycle, and W'_r is the weight of the retained oxide just before cooling, the spalling constant Q_0 is defined by:

$$F = Q_0 \cdot W_r^{\prime\alpha}$$

where α is an experimental constant, approximately equal to unity. From this formulation, various outputs of the COSP cyclic-oxidation model can

Table I. Chemical Composition of IN-625

Elements	Ni	Cr	Fe	Mo	Nb	Ta	Mn	Si	Ti	Al
W%	Base	22	5	9	3.15	3.15	0.5	0.5	0.4	0.4

be obtained, the total amounts of oxygen and metal reacted, the weight of retained oxide before and after spallation, the total amount of oxide spalled and the fractional amount of oxide spalled per cycle.

The purpose of this work was to study the performance of Inconel 625 under cyclic-oxidation conditions and then predict long-term behavior using the Cyclic Oxidation Spalling Program (COSP).

EXPERIMENTAL PROCEDURES

The chemical composition of superalloy Inconel 625 used in this study is given by Table I. Specimens were cut, having dimensions of $14 \times 9 \times 3$ mm. The coupons were polished with SiC papers up to 600 grit; then, they were ultrasonically washed in acetone.

The cyclic-oxidation tests consisted of holding the samples for 1 hr in a classical Eurotherm 818 furnace (Fig. 1), in air under atmospheric pressure, at the oxidation temperature followed by cooling (air quenching) for 30 minutes. The repeated thermal treatments are described by Fig. 2. The first level $p_r(1)$ consists of reaching the desired temperature from the minimum temperature. It requires a time not significant compared to a dwell time. The second level which presents more interest is the first dwell $p_d(1)$,

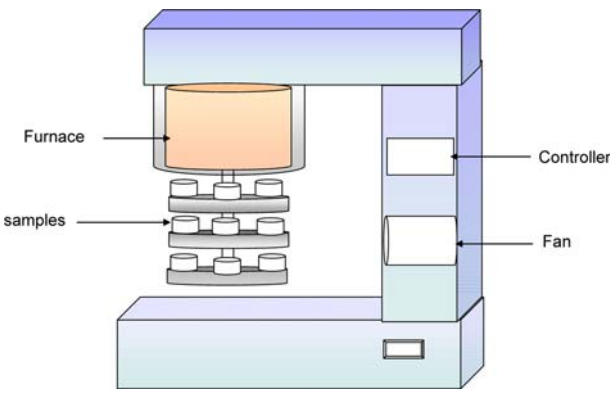

Fig. 1. Schematic representation of the cyclic oxidation furnace.

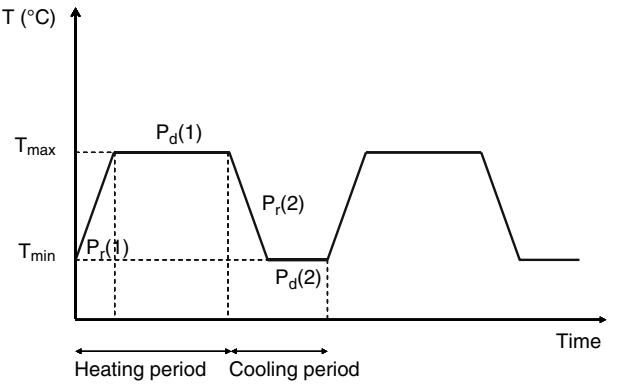

Fig. 2. Schema of thermal cycles applied in this study.

when the furnace is at the operating temperature. The ramp $p_r(2)$ describes the beginning of cooling up to the second dwell level $p_d(2)$ which indicates the minimum temperature of specimens. The experiments were carried out at 900 and 1000°C. The oxidized specimens were weighed to determine the net mass gain. Oxide morphology and spalls areas were characterized using scanning-electron microscopy (SEM) coupled with energy-dispersive analysis (EDS). X-ray diffraction (XRD) analyses were performed to determine the oxide composition.

RESULTS AND DISCUSSION

In order to study the cyclic-oxidation resistance of Inconel 625, this superalloy was subjected to laboratory cyclic-oxidation tests at 900 and 1000°C. The number of cycles was limited to 200. Characterization of a few samples oxidized for a number of cycles less than 200 was also made.

Influence of Oxidation Temperature

The specimen net weight gains obtained at 900 and 1000°C were plotted as a function of the cycle number (Fig. 3). The evolution of the kinetics curves obeys the parabolic growth law. An exception was noted for the kinetics at 1000°C where a process of mass loss, mass gain begins after 50 hrs. The oxidation rate is higher at 1000°C than that at 900°C.

The SEM images of Fig. 4 present the morphologies of oxides formed on Inconel 625 after 200 cycles at 900 and 1000°C. The oxide scale obtained

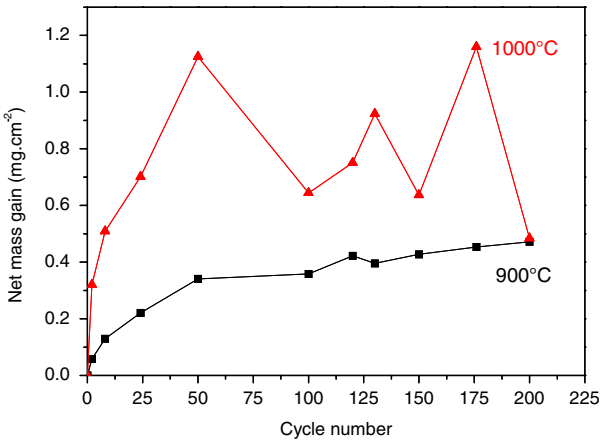

Fig. 3. Experimental kinetics curves, oxidation in air; 1 hr cycle, 900 and 1000°C.

at 900°C present a homogenous surface which is mainly a compound of spherical oxide grains. To the contrary, the oxide formed at 1000°C exhibits an outer surface covered by wider nodules. The cross section image, Fig. 5a, shows a thinner scale, about 2.5 μm at 900°C with a wavy metal-oxide interface. The associated mapping revealed the presence of chromium oxide. At 1000°C, Fig. 5b, the thicker oxide (12 μm) has an inner porous scale. Here, internal oxidation is more significant. The energy-dispersive-spectrometry analysis reveals in addition to chromium and oxygen, the presence of manganese and niobium at higher temperature. This result is in a good agreement with the corresponding mapping. The x-ray diffraction analyses, Fig. 6, confirm these observations. The corrosion product at 900°C is

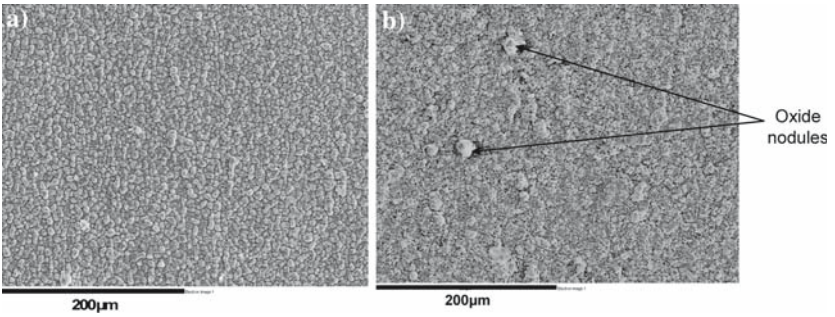

Fig. 4. SEM images of IN-625 after 200 cycles. (a) 900°C, (b) 1000°C.

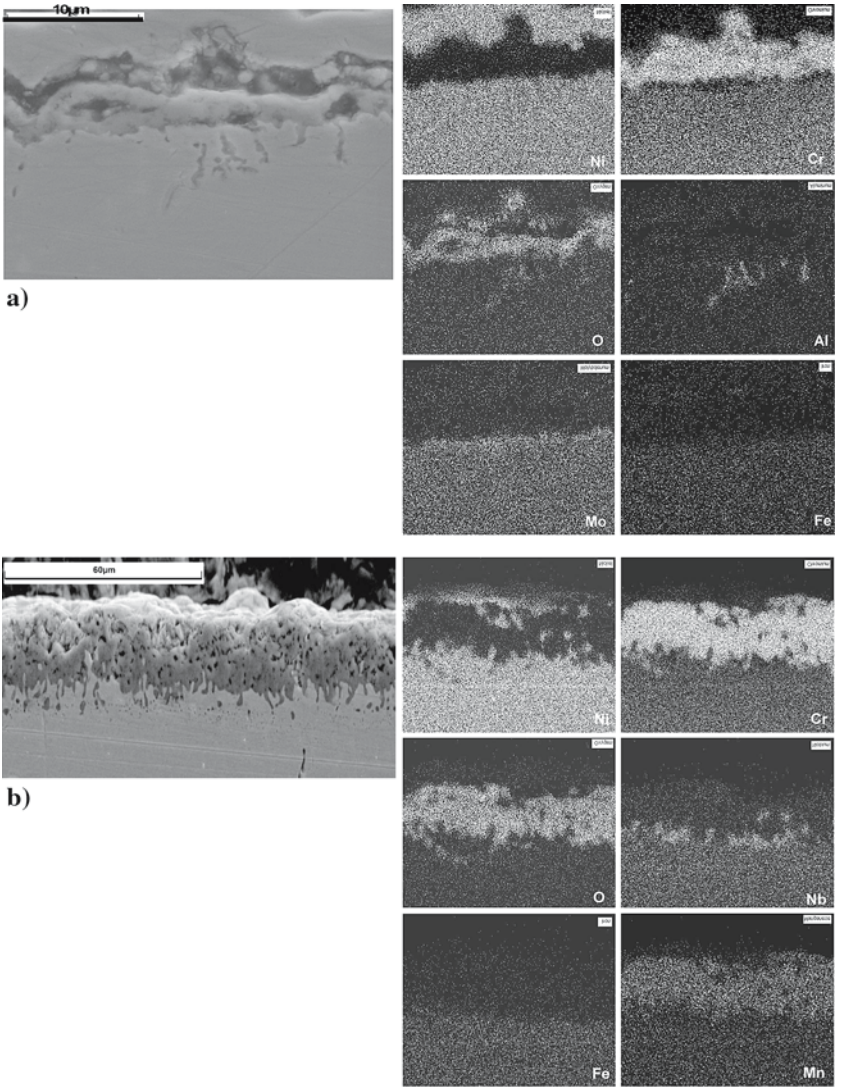

Fig. 5. SEM cross-section micrograph of IN-625 after 200 cycles. (a) 900°C, (b) 1000°C.

chromia with slight traces of molybdenum oxide, whereas at 1000°C the oxide scale consists of chromia and chromium manganese spinel.

The kinetics curves clearly show a higher weight gain at 1000°C, Inconel 625 exhibits a higher oxidation rate at high temperature as do other Ni-base superalloys[10] and stainless steels.[17] At 1000°C, mass loss and mass

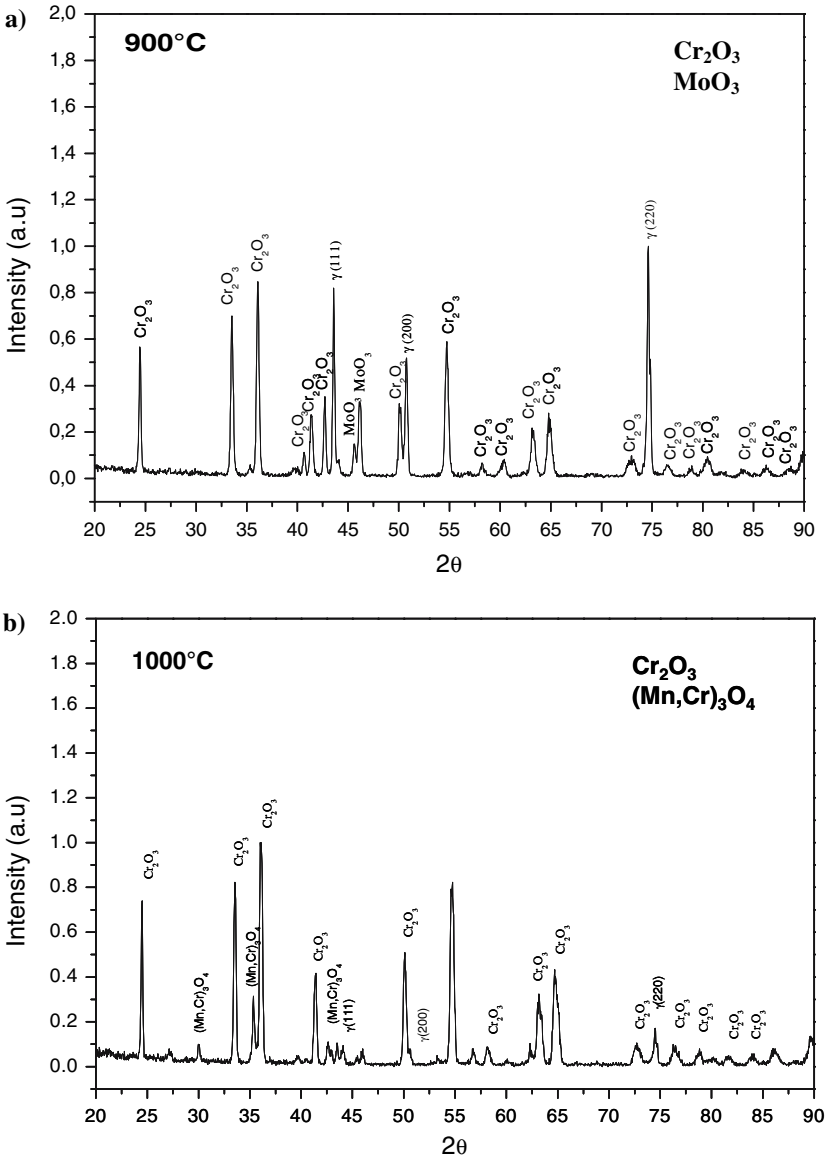

Fig. 6. XRD Diffractogram of oxide scale formed on IN-625 at (a) 900°C and (b) 1000°C.

gain occur after 50 hrs exposition in air. This phenomenon is probably due to chromium evaporation and/or spallation followed by reoxidation. The reoxidation can lead to rapid chromium consumption which can result

in breakaway oxidation.[13,18,19] The chromium-evaporation rate starts at a value about $2.67 \cdot 10^{-8}$ Kg m^{-2} s^{-1}. This value increases with time as illustrated by the slope of the mass-loss curve at 150 and 200 cycles. The volatilization of CrO_3 (g), which is the most-prevalent chromium-oxide-gas species in dry air,[3,20] reduces the diffusion distance through the oxide compared to a more-stable oxide; then accelerated corrosion attack occurs. That explains very well the process of mass gain after each chromium evaporation observed in Fig. 3. The porous scale is due mainly to CrO_3 (g) volatilization which promotes inward oxygen diffusion which results in internal oxidation. The internal oxidation causes interfacial-chromium depletion which is detrimental for the superalloy. Internal oxides in the metal can act as crack initiators or stress concentrators, leading to scale spallation.[21] At 1000°C, $(Mn,Cr)_3O_4$ spinel formation, due to the higher diffusivity of Mn, two orders of magnitude greater than the other lattice-diffusion coefficients (Cr, Fe, Ni),[9] is beneficial for the oxide scale at this temperature. Manganese–chromium spinel improves oxide adherence as mentioned by Perez et al.[22] and probably reduces the chromium-evaporation rate. This last beneficial effect of alloying element such Mn was studied widely by Holcomb and Alman.[20] They demonstrated that the $MnCr_2O_4$ spinel formation by Mn additions reduces the Cr_2O_3 activity and consequently lowers the vapor pressure of CrO_3(g). At 900°C, there is no manganese–chromium spinel formation, however the oxide scale, thinner than that at 1000°C, remains continuous and more adherent up to 200 cycles, and no chromium evaporation occurred. Superalloy IN-625 exhibits a better cyclic oxidation resistance at this temperature.

Influence of Exposure Time (cycle number)

At 1000°C, the corrosion products were characterized after 24, 130 and 200 cycles. The SEM images presented in Fig. 7 show the development of oxide grains, the growth of superficial nodules in number and size when the cycle number increases. Alloying elements such Mn, Ti and Nb were distributed on the oxide scale surface as illustrated by the EDS spectrum.

The X-ray diffractograms of Fig. 8 give the phases of oxide scales formed at the three times, chromia and manganese–chromium spinel. The peaks of the matrix (γ) decrease when the cycle number increases. The oxide scale thickens with increasing oxidation time. Cr_2O_3 and $(Mn,Cr)_3O_4$ which normally constitute a protective diffusion barrier, exist in the form of nodules. The development of these later with time toward the surface and the vacancy condensation due to outward-cation diffusion and inward diffusion of vacancies may lead the establishment of cavities and pores at the

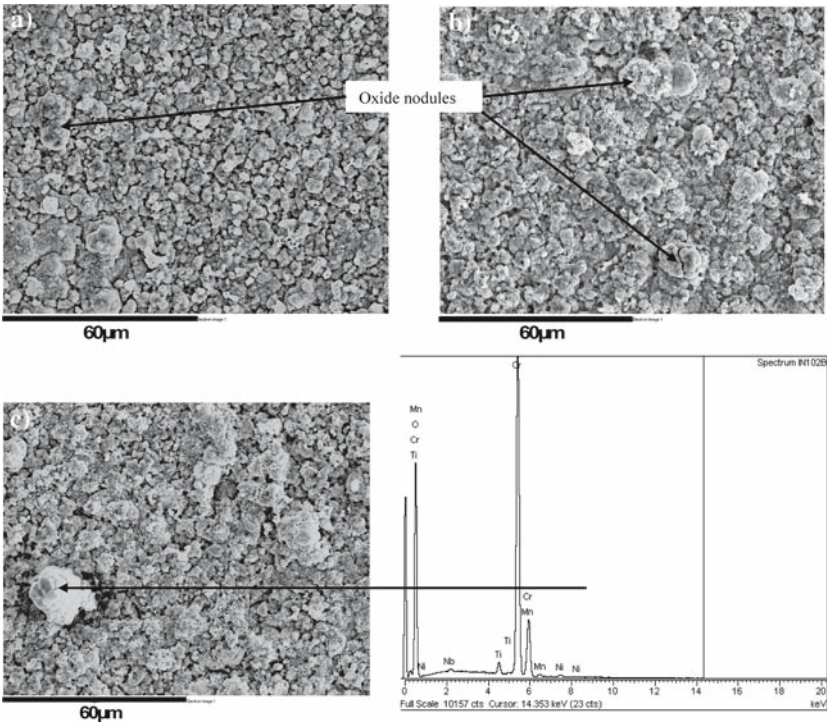

Fig. 7. SEM surface image of oxide formed on IN-625 at 1000°C. (a) 24 hr, (b) 130 hr and (c) 200 hr.

oxide-metal interface;[23] where the oxygen partial pressure increases. This resulted in internal oxidation which was observed after 200 cycles. The oxide scale obtained after 200 hrs is more porous than that formed after 24 hrs. Long-term exposure seems to be detrimental. The chromia scale losses its protective property and then IN-625 exhibits lower cyclic-oxidation resistance.

Cyclic Oxidation Behavior: Simulation with the COSP Model

The experimental data from cyclic oxidation at 900 and 1000°C of superalloy IN-625 were calculated using the COSP model. The computer-simulation result is presented in Fig. 9. Because of evaporation of chromium oxide, the simulation was limited at 50 cycles for specimens oxidized at 1000°C. After 50 cycles, the oxide did not grow following the parabolic law. So we put more interest on the behavior at 900°C. As indicated in the first

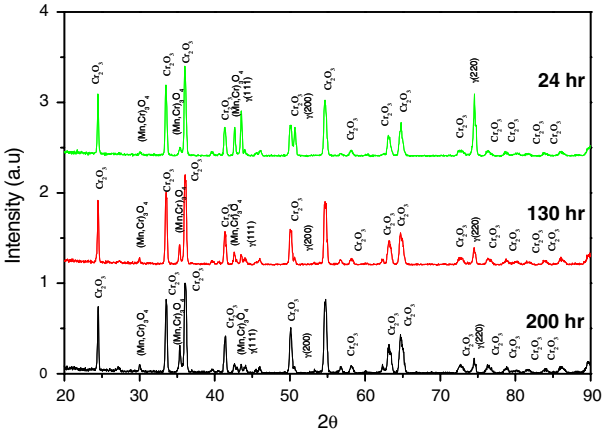

Fig. 8. XRD Diffractogram of oxide scale formed on IN-625 at 1000°C during 24 hr, 130 hr and 200 hr.

part, above, the parabolic growth rate was greater at 1000°C than that at 900°C, $3 \cdot 10^{-2}$ and $2 \cdot 10^{-3}$ $mg^2\ cm^{-4}\ h^{-1}$, respectively. The model curves (solid lines) fit very well the experimental data (Fig. 9). Apart from the parabolic rate constant (k_p) and spall constant (Q_0), the model fit other parameters for the two temperatures (same oxide Cr_2O_3): stoichiometric constant: 3, 1666; spall exponent α:1 and spall case:uniform thickness. There was no spallation until the end the test (oxidation at 900°C). So we tried to

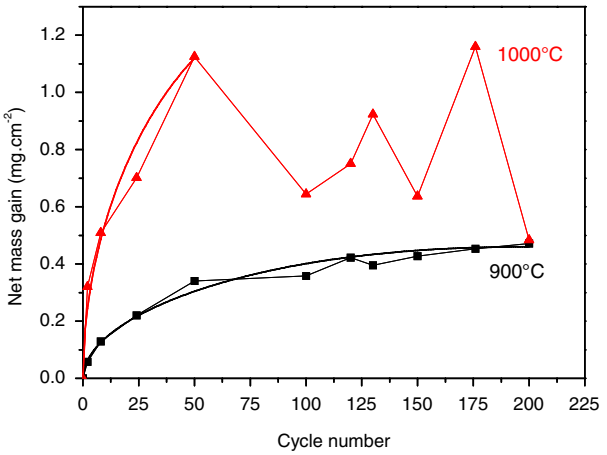

Fig. 9. COSP model curves and experimental data of IN-625 oxidized in air at 900 and 1000°C (200 cycles).

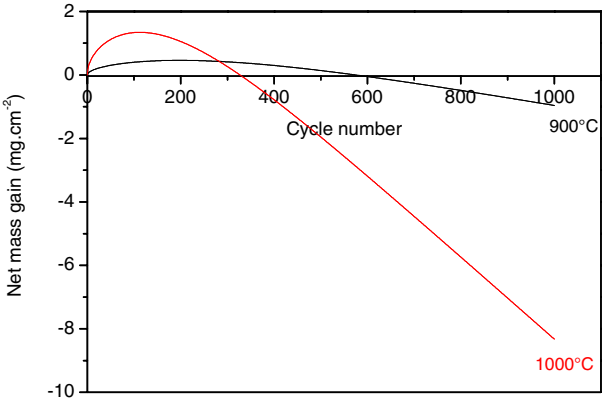

Fig. 10. COSP model curves of IN-625 oxidized in air at 900 and 1000°C (1000 cycles).

simulate the cyclic-oxidation behavior of IN-625 for long-time exposure, 1000 cycles. The model curves of Fig. 10, without evaporation, confirm the best performance of the superalloy at 900°C. The features of the thermal treatment at both temperatures are summarized in Table II. At higher temperature, the metal reach rapidly the maximum weight change, followed by a decrease to zero weight change at 327 cycles and a final linear rate of loss. To the contrary the time to cross zero weight change for a specimen oxidized at 900°C was 575 hrs. The protective effect of the oxide formed on IN-625 appears up to about 600 hrs under cyclic-oxidation conditions at 900°C.

CONCLUSION

The cyclic-oxidation tests performed on Superalloy IN-625 clearly showed a difference of morphology of oxide scale formed at 900 and 1000°C. The lower temperature promotes a homogenous scale which is mainly

Table II. Computer-Simulation Features, after 1000 Cycles

	k_p(mg^2 cm^{-4} h^{-1})	Q_0	Maximum weight change (mg cm^{-2})	Time to reach maximum weight change (hr)	Cycles to reach crossover	Weight of metal consumed (mg cm^{-2})
900°C	0.002	$50 \cdot 10^{-5}$	0.46	197	575	3.64
1000°C	0.030	$30 \cdot 10^{-5}$	1.34	112	327	16.24

protective chomium oxide. No spallation was observed after 200 cycles. The oxide scale obtained at 1000°C was a mixture of chromia and chromium–manganese spinel. At 1000°C, the evaporation of chromium-oxide gas enhanced the growth of voids and cavities leading to an inner porous scale which resulted in faster internal oxidation. Long-term exposure also leads to microstructural modification. The cyclic-oxidation behavior simulated by the COSP program confirmed the better performance of IN-625 at 900°C. For 1000 cycles, the predicted data project a time to cross-over of IN-625 up to 600 hrs, according to a negative-weight criterion.

ACKNOWLEDGEMENTS

The authors want to express their gratitude to Dr. J. Smialek from NASA for the COSP computer program.

REFERENCES

1. N. Vialas, D. Monceau, and B. Pieraggi, *Material Science Forum* **461–464**, 747 (2004).
2. B. A. Pint, *Surface and Coatings Technology* **188–189**, 71 (2004).
3. C. T. Liu, X. F. Sun, H. R. Guan, and Z. Q. Hu, *Surface and Coatings Technology* **197**, 39 (2005).
4. L.Geng, Y. S. Na, and N. K.Park, *Materials and Design* (2006), in press (corrected proof).
5. T. S. Sidhu, S. Prakash, and R. D. Agrawal, *Scripta Materialia* **55**, 179 (2006).
6. P. Berthod, S. Michon, J. D. Martino, S. Mathieu, S. Noël, R. Podor, and C. Rapin, *Computer Coupling of Phase Diagrams and Thermochemistry* **27**, 279 (2003).
7. Y. J. Xie, M. C. Wang, G. Zhang, and M. Chang, *Engineering Failure Analysis* **13**, 1429 (2005).
8. L. Jian, C. Y. Yuh, and M. Farooque, *Corrosion Science* **42**, 1573 (2000).
9. F. Riffard, H. Buscail, E. Caudron, R. Cueff, C. Issartel, and S. Perrier, *Corrosion Science* **45**, 2867 (2003).
10. J. H. Luo, Q. Zhang, and F. B. Song, *Computation Materials Science* **31**, 220 (2004).
11. J. L. Smialek, J. A. Nesbitt, C. A. Barrett, and C. E. Lowell, *European Federation of Corrosion* **27**, 148 (1999).
12. S. Osgerby, K. Berriche-Bouhanek, and H. E. Evans, *Materials Science and Engineering A* **412**, 182 (2005).
13. B. Gleeson, and B. Li, *Material Science Forum* **461–464**, 427 (2004).
14. J. L. Smialek, *Acta Materialia* **52**, 2111 (2004).
15. J. L. Smialek, *Acta Materialia* **51**, 469 (2003).
16. J. L. Smialek, and J. V. Auping, *Oxidation of Metals* **57**(5/6), 559 (2002).
17. R. Yin, *Materials Science and Engineering A* **391**, 19 (2005).
18. B. A. Pint, and I. G. Wright, *Journal of Nuclear Materials* **307–311**, 763 (2002).
19. F. Riffard, H. Buscail, E. Caudron, R. Cueff, C. Issartel, and S. Perrier, *Applied Surface Science* **252**, 3697 (2006).
20. G. R. Holcomb, and D. E. Alman, *Scripta Materialia* **54**, 1821 (2006).
21. B. A. Pint, J. R. DiStefano, and I. G Wright, *Materials Science and Engineering A* **415**, 255 (2006).

22. F. J. Pérez, M. J. Cristóbal, M. P. Hierro, and F. Pedraza , *Surface and Coatings Technology* **120–121**, 442 (1999).
23. D. Oquab, and D. Monceau, *Scripta Materialia* **44**, 2741 (2001).